Article

A Novel Reduced Reaction Mechanism for Diesel/2,5-Dimethylfuran Engine Application

Song Li [1],*, Wenbin Yu [1], Chen Yang [1], Mingrui Wei [2] and Jinping Liu [1]

1   School of Mechanical Engineering, Anyang Institute of Technology, Anyang 455000, China
2   School of Automotive Engineering, Wuhan University of Technology, Wuhan 430070, China
*   Correspondence: 20180030@ayit.edu.cn

Abstract: The application of 2,5-dimethylfuran (DMF) as an alternative fuel for internal combustion engines has been gaining popularity. However, it has rarely been studied in previous research on the chemical kinetics of DMF for engine combustion simulations. In the present study, a reduced n-heptane/toluene/DMF-polycyclic aromatic hydrocarbon (PAH) reaction mechanism containing only 78 species amongst 190 reactions was proposed and applied to predict the combustion and emissions of a diesel engine using diesel/DMF blend fuel. First, a detailed reaction mechanism for DMF from the literature was chosen and reduced using combined mechanism reduction methods under engine-relevant conditions. Second, the reduced mechanism of DMF was incorporated into an existing reduced n-heptane/toluene-PAH mechanism to establish a three-component chemistry mechanism. Third, the predictive capability of the combined mechanism was improved by adjusting the rate constants of selected gas-phase reactions. Subsequently, the proposed three-component mechanism was compared and validated with experimental measurements of shock tube ignition delay times and premixed flame species profiles acquired from published papers. Moreover, new experimental data from a conventional diesel engine were used to evaluate the developed mechanism. Overall, the predicted results obtained by this proposed reduced n-heptane/toluene/DMF-PAH mechanism are in reasonable agreement with the available experiments.

Keywords: 2,5-dimethylfuran; n-heptane; toluene; reaction mechanism; diesel engine

1. Introduction

Fossil fuel depletion and environmental degradation raise more public concerns over the employment of alternative fuels to replace diesel and gasoline. Biodiesel is identified to be an effective replacement for diesel fuel [1,2], but this fuel has some significant drawbacks, such as high energy consumption during its production, susceptibility to oxidation and poor low-temperature properties [3]. Moreover, biodiesel combustion usually produces more nitric oxides (NOx) [4]. Ethanol has long been considered as a gasoline alternative that can also be used as additive in diesel fuel. Nonetheless, its application is limited by low energy density, high production cost, high volatility and high miscibility with water [5]. Therefore, many studies have been carried out in search of improved alternative fuels to biodiesel and ethanol.

With deep research on biofuels, 2,5-dimethylfuran (DMF) has been receiving increasing interest as a promising alternative in internal combustion engines (ICEs) [6–11]. DMF can be produced in a high yield from glucose, fructose, sucrose, starch and cellulose [12,13]. Moreover, DMF has more favorable physicochemical properties compared to biodiesel or ethanol; as shown in Table 1 [14,15], the high octane number and boiling point of DMF are beneficial to restrain the engine knock and the vapor lock in the inlet. DMF has a high density and low latent heating value, which give the engine a better cold start performance. With about 16.7% oxygen content, DMF can generally improve the combustion process of the engine. Moreover, compared with ethanol, DMF has a higher energy density and

lower water solubility. Attracted by these advantages, DMF has been widely studied for its practical application in ICEs.

Table 1. Properties of diesel, gasoline, biodiesel, ethanol and DMF [14,15].

	Diesel	Gasoline	Biodiesel	Ethanol	DMF
Molecular formula	C_{12}–C_{25}	C_4–C_{12}	C_{12}–C_{24}	C_2H_5OH	C_6H_8O
Cetane number	40–55	10–15	52	8	–
Octane number	–	90–99	–	108	119
Oxygen content (wt %)	–	–	10	34.8	16.7
Density at 20 °C (g/cm^3)	0.820	0.745	0.880	0.790	0.890
Boiling point (°C)	180–370	25–215	262–359	78.4	92–94
Viscosity at 20 °C (mm^2/s)	4.8	0.4–0.8	8.9	1.08	0.65
Low heating value (MJ/kg)	42.5	42.7	38.0	26.8	33.7
Latent heating at 25 °C (kJ/kg)	270–301	380–500	320	904	333
Autoignition temperature (°C)	246	420	363	434	285.85
Stoichiometric A/F ratio	14.3	14.7	12.5	9.02	10.79

The employment of DMF as an alternative fuel or fuel additive for spark ignition (SI) engines has been evaluated in many engine studies. Zhong et al. [6] compared the combustion performance of a single-cylinder SI engine fueled with DMF, gasoline and ethanol, and the comparisons demonstrated that DMF offered similar combustion and emission levels in comparison with gasoline; thus, it can be used in existing SI engines without significantly modifying them. Daniel et al. [16] found that the combustion efficiency improved and the hydrocarbon (HC) and carbon monoxide (CO) emissions decreased when a single-cylinder SI engine used DMF as fuel. In addition, Daniel et al. [17] reported that DMF combustion yielded the lowest emission level of formaldehyde and carbonyl compounds compared to methanol, ethanol, n-butanol and gasoline. Comparisons were conducted by Shukla et al. [7] with an SI engine using pure gasoline, DMF/gasoline and ethanol/gasoline blends. They reported that the DMF/gasoline blend yielded a comparable performance and lower pollutant emissions than gasoline. Rothamer and Jennings [18] investigated the knocking propensity of a single-cylinder direct-injection (DI) SI engine fueled with DMF/gasoline and ethanol/gasoline mixtures at three load conditions. Their results indicated that the antiknock properties of gasoline were improved by the addition of both DMF and ethanol. Wang et al. [19] investigated the particulate matter (PM) component and soot oxidation characteristics of running gasoline, ethanol, ethanol/gasoline blend and DMF in a DI SI engine. Results revealed that soot particles produced from the combustion of ethanol and DMF were more susceptible to oxidation than gasoline soot.

DMF has also been demonstrated to be suitable for application in compression ignition (CI) engines. As the octane number of DMF is 119, its use should be as a diesel fuel additive, because it is difficult to ignite when a CI engine is fueled with pure DMF. Zhang et al. [20] and Chen et al. [21,22] pointed out that DMF addition could obviously extend the low pollutant emission region and improve the NOx-soot trade-off relationships without deteriorating fuel economy. In particular, the NOx-soot trade-off could be eliminated; meanwhile, soot particle emission was close to zero with a blending ratio up to 40%. In addition, CO and HC emission levels were not obviously affected. Compared with gasoline and n-butanol, DMF showed an advantage in reducing soot emissions because of the combined effects of its octane number and oxygen content. Liu et al. [23] compared four types of fuels (n-heptane, DMF, cetane/iso-cetane and DMF/2-ethylhexyl nitrate mixtures) in blending with diesel, respectively, with 20% blending proportion on a CI engine. They concluded that DMF addition showed the lowest soot emission and higher NOx emission among tested fuels, but it had little impact on the emissions of HC and CO. Zheng et al. [8] experimentally compared six types of fuels added into diesel with same oxygen content in a single-cylinder CI engine. Their findings revealed that DMF was more effective to improve the engine performance compared to 2-hexanone, n-hexanol, cyclohexanone, cyclohexanol and isopropyl ether. Recently, Xiao et al. [9,24] presented results of the combustion and emission performances of diesel/DMF mixtures on a DI CI

engine at few loads. Their findings revealed the acetaldehyde emission increased with the addition of DMF, while the emissions of benzene and 1,3-butadiene were diminished. Moreover, DMF addition tended to reduce the mass and number of concentrations of PM under most operating conditions. The experiments of Wei et al. [10,11] found that diesel/DMF blends could improve the brake thermal efficiency and decrease the number of large particles and the particle diameter but increase the number of small-size particles. Wang et al. [25] experimentally investigated the morphology, nanostructure and reactivity of soot particles produced from diesel/DMF blends on a CI engine. The finding portrayed that DMF addition could decrease the diameter and fringe length of primary particles but increase the fringe tortuosity. In addition, soot particles from the combustion of blend fuels were more reactive to oxidation than diesel soot due to their more disordered nanostructure.

As mentioned above, the use of DMF as alternative fuel or fuel additive in ICEs is getting more widespread. However, most previous studies conducted regarding the application of DMF fuel in CI engines were experimental, and there are few numerical studies that have been reported. A reduced reaction mechanism for diesel/DMF combustion containing the formation of polycyclic aromatic hydrocarbon (PAH) was proposed by Liu et al. [14] for CI engine applications, in which n-heptane was employed to represent diesel fuel. The mechanism involves 136 species and 617 reactions and its performance was well evaluated by comparing experimental values. A reasonable match between the simulations and experiments could be obtained. It should be noted that the diesel/DMF mechanism should be further downsized so that it can be employed in multidimensional engine simulations more efficiently. In addition, it is well known that diesel fuel is composed of hundreds to thousands of compounds; in particular, the aromatic class of compounds play a significant role in forming soot particles. The study by Weber et al. [26] indicated that n-heptane combustion yields lower soot emissions compared to diesel because of the lack of aromatic compounds. Therefore, it is reasonable to expect that diesel surrogate fuel is represented by a mixture composed of two or more components.

This work focuses on the development of a reduced three-component chemistry mechanism, consisting of n-heptane, toluene and DMF, suitable for use in three-dimensional simulations of CI engine combustion and emissions, in which a 70% n-heptane and 30% toluene mixture is employed to represent diesel fuel. A detailed DMF mechanism proposed by Tran et al. [27] was reduced firstly, and then merged into a n-heptane/toluene-PAH mechanism developed in our previous work [28] to form a combined mechanism. After that, the reduced combined mechanism was optimized and extensively assessed by comparison with available experimental results from shock tubes and laminar premixed flames. Furthermore, the in-cylinder combustion and engine-out emissions of diesel/DMF fuels were experimentally studied on a four-cylinder CI engine, and the corresponding measured data were employed to further assess the proposed mechanism.

2. Kinetic Model Construction

2.1. The Reduced DMF Mechanism

A detailed DMF oxidation model developed by Tran et al. [27], consisting of 379 species amongst 2204 reactions, was selected as the starting mechanism for the reduction. The direct relation graph error propagation (DRGEP) method [29] was firstly employed for the mechanism reduction. This method is used to eliminate the least coupled species by using a directed graph approach, during which process the resulting propagation error due to the removal of the corresponding species is still restrained to be within a specified value. Details about the DRGEP method can be found in Ref. [29]. This reduction process for the detailed DMF mechanism was performed by considering the equivalence ratios (φ) of 0.5–2.0, pressures of 1–80 bar and temperatures of 800–1600 K, which are similar to the working conditions of ICEs. Meanwhile, the target species were DMF, O_2, nitrogen (N_2), carbon dioxide (CO_2), water (H_2O), CO and hydrogen (H_2). After the DRGEP process, the computational singular perturbation (CSP) method [30] was utilized to further remove unimportant reactions under same conditions as the first stage. The

normalized contribution of reaction to the net production rate of a species was computed by the CSP method based on the iterative threshold within a user-specified limit, below which the reaction was considered unimportant and removed from the mechanism. At each reduction step, the performance of the generated reduced mechanism was compared with the starting mechanism to ensure it retained acceptable predictive power. Following the automatic reduction process, manual reductions were carried out using the methods of rate of production analysis (ROPA), temperature sensitivity analysis (SA) and chemical lumping to further lessen the size of the generated mechanism. The important species and reactions could be identified by employing the manual reduction methods, which were considered retainable. Finally, a reduced mechanism comprising 65 species and 159 reactions for DMF oxidation was constructed.

A reaction path analysis of the reduced DMF mechanism at 1200 K and simulation time corresponding to around 20% fuel conversion was conducted in a homogeneous batch reactor for an ignition process of stoichiometric DMF/air mixture at 40 bar pressure, as shown in Figure 1. There are four main consumption pathways of DMF. The primary fuel consumption pathway for DMF is H abstraction reactions initiated by the O_2, OH, H and CH_3 radicals, producing the methyl group, forming the 5-methyl-2-furanylmethyl radical ($R1C_6H_7O$) (~61.82%). Then, $R1C_6H_7O$ undergoes decomposition reactions, generating cyclopentadienyl (C_5H_5) and C_3H_4. A second important pathway of DMF consumption is ipso-addition reactions to yield 2-methylfuran (MF) (~18.23%). Another channel of consumption of DMF (~12.89%) is attacked by the H-atom to form the 1,3-butadiene (C_4H_6) and acetyl radical (CH_3CO). Furthermore, acetylene (C_2H_2), CH_3CO and acetaldehyde (CH_3CHO) can be produced via OH addition to the C2 position of DMF.
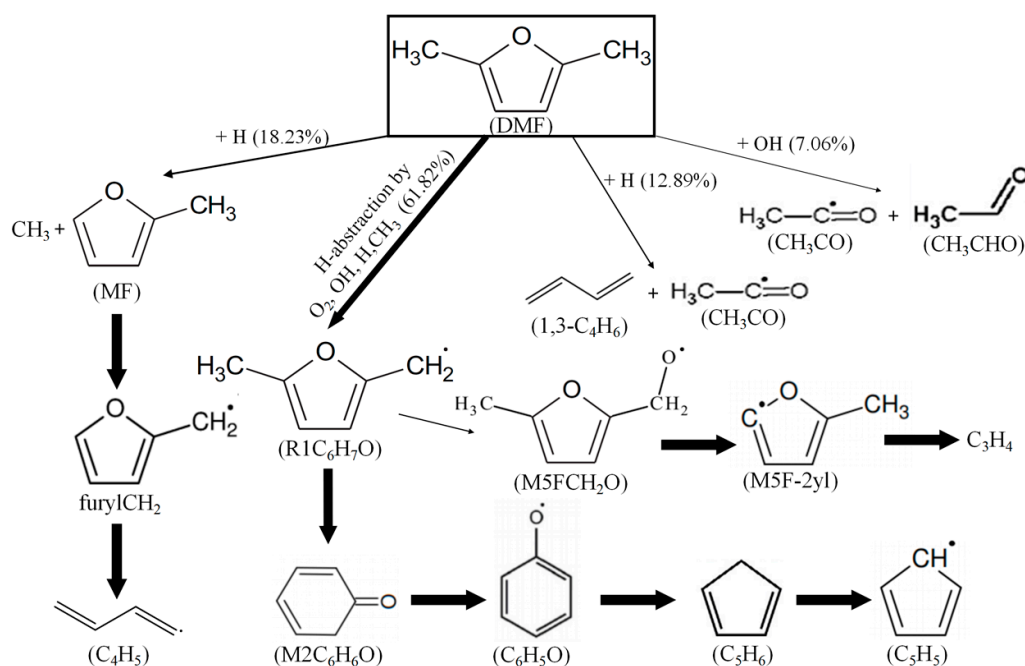
Figure 1. Reaction path analysis for DMF combustion after 20% fuel consumption at 40 bar and 1200 K. The size of the arrows is proportional to the relative rates of consumption of a given species.

2.2. The Combined Mechanism

The reduced mechanism of n-heptane and toluene with PAH formation proposed by our previous work [28] was adopted as the base mechanism of diesel/DMF mechanism. This reduced mechanism involves only 69 species amongst 178 reactions, in which a 70% n-heptane and 30% toluene mixture was utilized as surrogate for diesel fuel, because it is able to well represent the cetane number and other properties of real diesel fuel [31,32]. This reduced diesel surrogate fuel mechanism has been extensively assessed through ignition delays, speciation profiles and diesel engine modeling and gives a reasonable prediction.

A combined n-heptane/toluene/DMF-PAH mechanism, which contains 78 species amongst 190 reactions, was formulated by integrating the DMF submechanism into the base mechanism. During the process of mechanism merging, the cross reactions between DMF and the other two components were not considered due to the interactions among large fuel compounds being unimportant [33–35]. Meanwhile, in order to preserve the integrity of the diesel surrogate fuel mechanism, duplicated species and reactions in the diesel surrogate fuel mechanism were retained. The three-component chemistry mechanism contains three levels, i.e., the fuel consumption (C_n-C_4, from raw fuel to C_4 species) reactions, the H_2/CO/C_1-C_3 reactions and the PAH formation reactions.

2.3. Optimization of the Combined Mechanism

After the merge process, the simulated ignition delay times and flame species profiles using the combined mechanism deviated obviously from those of the measurements. Therefore, the combined mechanism needs to be optimized to improve its predictive ability. Firstly, the autoignition behaviors of three fuel compounds were validated by comparing the predictions and experimental results from shock tubes. According to the deficiencies of the present mechanism in predicting ignition delays, the SA method was used to verify the most sensitive reactions related to shock tube measurements. The rate constants of selected reactions were modified by optimizing the pre-exponential factors to achieve better agreement with experimental ignition delays over wide operating conditions. Secondly, in order to make sure that the proposed mechanism could provide satisfactory predictions of the primary flame species concentrations, similar procedures were conducted by using the path analysis and ROPA methods to calibrate the pre-exponential factors of the crucial reactions. Thirdly, the above two procedures were carried out iteratively until an acceptable tolerance between the predictions and measurements was achieved. The optimized reactions with their corresponding pre-exponential factors are listed in Table 2. The reduced n-heptane/toluene/DMF-PAH mechanism in CHEMKIN format is included in the Supplementary Material.

Table 2. Adjusted A factors for n-heptane/toluene/DMF-PAH mechanism.

| Reactions	Original A Factor	Adjusted A Factor
$C_7H_{16} + HO_2 = C_7H_{15}$-$2 + H_2O_2$	1.00×10^{13}	5.00×10^{13}
$C_7H_8 + O_2 = C_7H_7 + HO_2$	3.00×10^{14}	5.00×10^{14}
$C_7H_8 + H = C_7H_7 + H_2$	1.50×10^{14}	1.50×10^{13}
$DMF + O_2 = R1C_6H_7O + HO_2$	4.20×10^{12}	8.40×10^{13}
$DMF + H = R1C_6H_7O + H_2$	3.10×10^5	5.10×10^5
$DMF + OH => CH_3CO + CH_3CHO + C_2H_2$	7.95×10^{12}	7.95×10^{10}
$DMF + H = CH_3CO + C_4H_6$	1.34×10^{32}	5.34×10^{32}
$R1C_6H_7O + HO_2 = M5FCH_2O + OH$	5.00×10^{12}	5.00×10^{13}
$C_4H_4 + OH = C_4H_3 + H_2O$	1.00×10^7	1.00×10^9
$C_4H_3 + H = C_2H_2 + C_2H_2$	6.30×10^{25}	8.30×10^{25}
$C_4H_4 + C_2H_3 = A_1 + H$	1.90×10^{12}	1.90×10^{14}
$C_3H_3 + C_3H_3 = A_1$	2.00×10^{12}	2.00×10^{14}
A_1- $+ C_4H_2 = A_2$-1	5.10×10^{48}	5.10×10^{50}
A_2-$1 + C_2H_2 = A_2R_5 + H$	1.10×10^7	1.10×10^6
$A_1C_2H + A_1$- $= A_3 + H$	1.10×10^{23}	3.10×10^{23}
$O + OH = O_2 + H$	2.04×10^{14}	8.04×10^{13}

3. Mechanism Validation

3.1. Ignition Delay Times

Ignition delays predicted by the proposed n-heptane/toluene/DMF-PAH mechanism are compared and validated against measurements available from literature in this section. The SENKIN code in the CHEMKIN package [36] was used to simulate the ignition delays in shock tubes. Figure 2 shows the predicted and experimental ignition delays of n-heptane/air at φ of 1.0 and 2.0 and temperatures of 650–1250 K; the experimental results

were obtained from Ciezki et al. [37] and Hartmann et al. [38]. As seen, the ignition delays of n-heptane/air have evident negative temperature coefficient (NTC) phenomena between 750 K and 950 K. In general, the proposed mechanism can well reproduce the experimental measurements over a wide temperature range at different equivalence ratios and pressures, capturing the characteristic of NTC regions and the reduction in ignition delays with increasing initial pressure.
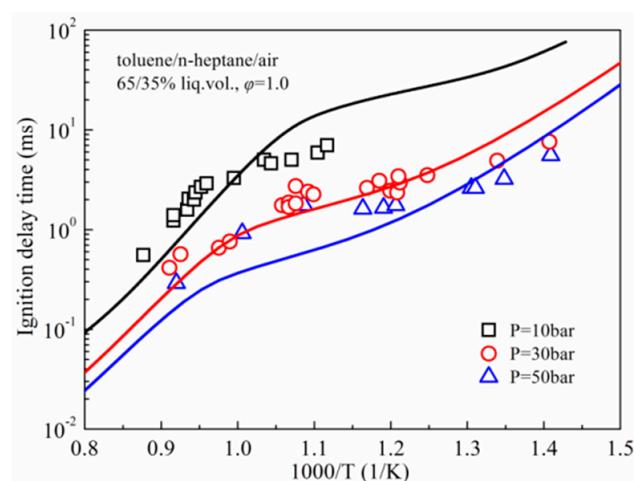

(a) $\varphi = 1.0$ (b) $\varphi = 2.0$
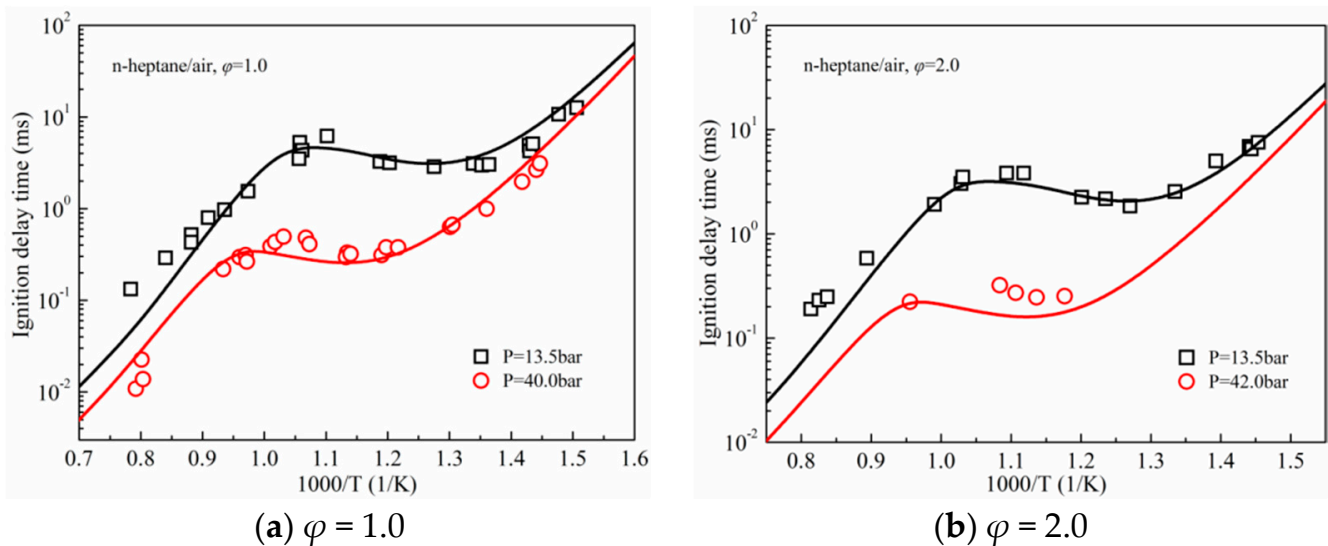
Figure 2. Comparisons between the predicted (lines) and experimental [37,38] (symbols) ignition delays of n-heptane/air mixtures.

Ignition delays of toluene/air mixtures at 50 bar and temperatures of 855–1400 K for two different equivalence ratios (φ= 0.5 and 1.0) in a reflected shock tube were reported by Davidson et al. [39] and Shen et al. [40]. Figure 3 depicts comparisons of measured and calculated ignition delay times of toluene/air mixtures by the proposed mechanism. As seen, both the measured and calculated shock tube results reveal that the ignition delays of toluene show a linear behavior relative to temperature, and there is no NTC behavior is observed. Overall, the predicted results obtained by the proposed mechanism satisfied the measured data.

(a) $\varphi = 0.5$ (b) $\varphi = 1.0$
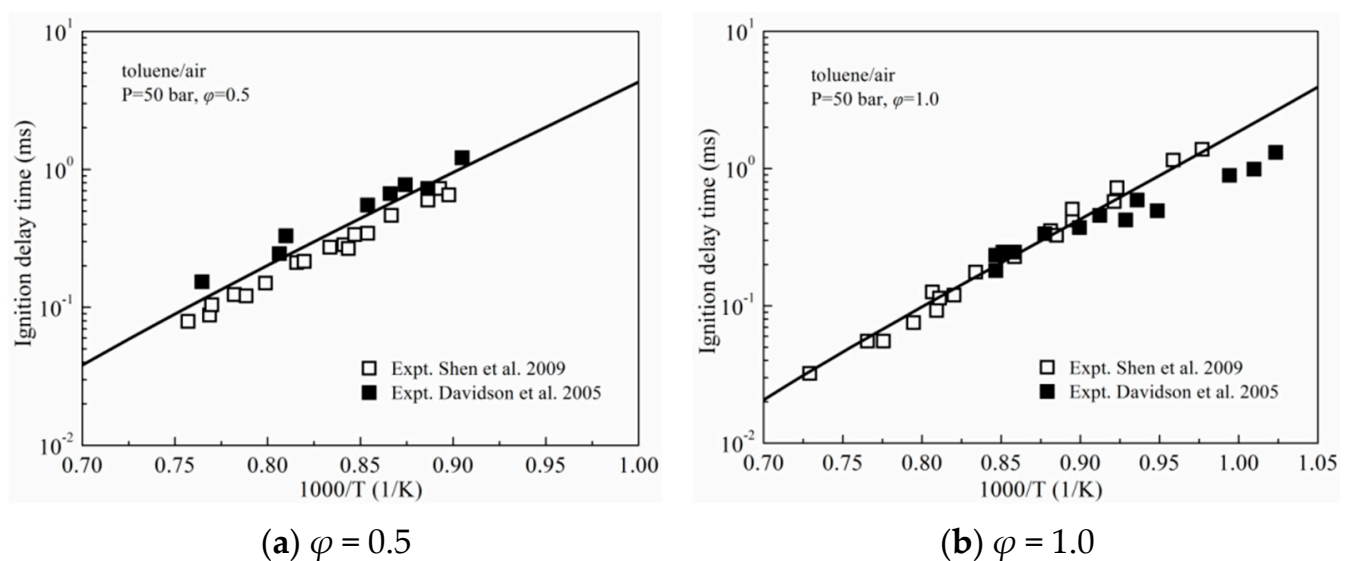
Figure 3. Comparisons between the predicted (lines) and experimental [39,40] (symbols) ignition delays of toluene/air mixtures.

The ignition delays for a stoichiometric mixture consisting of 35% n-heptane and 65% toluene by liquid volume were determined by Herzler and his coworkers [41] in a high-pressure shock tube at pressures of 10, 30 and 50 bar and temperatures of 620–1180 K. Figure 4 depicts comparisons of ignition delay predictions and shock tube experimental results. As shown, both the measured and predicted results reveal that the ignition delays decrease with the increase in pressure. The proposed mechanism can capture the variation trends of the shock tube experimental results, and can also reproduce the measurements reasonably well under different initial pressure conditions with a maximum deviation of two to three times.
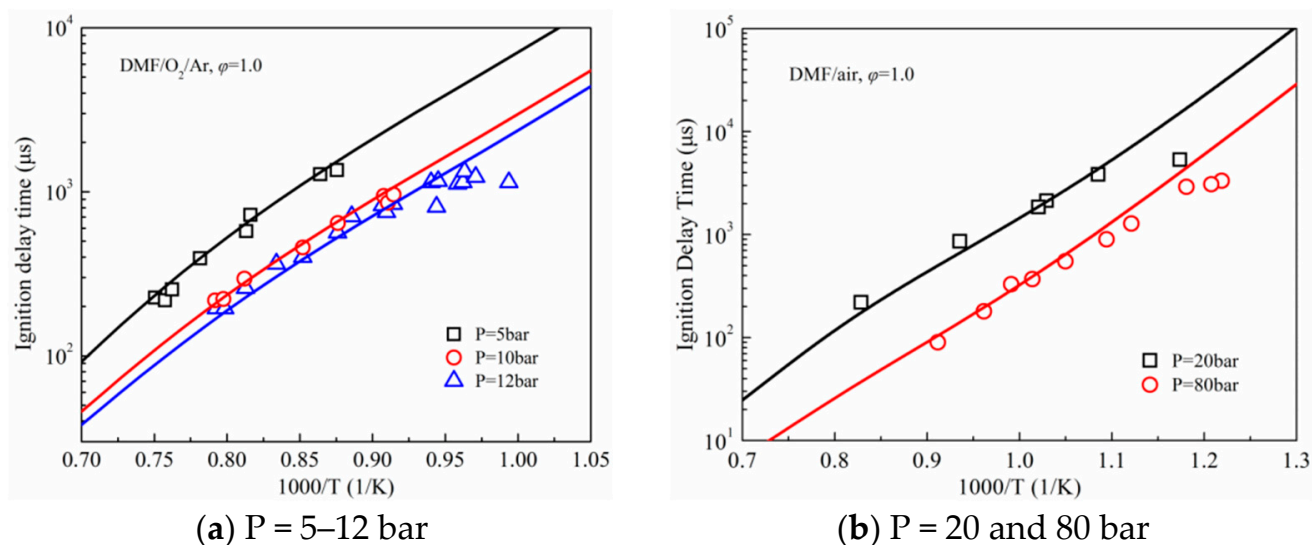

Figure 4. Comparisons between the predicted (lines) and experimental [41] (symbols) ignition delays of n-heptane/toluene/air mixtures.

The shock tube experimental data for stoichiometric DMF in argon (Ar)-diluted oxygen mixture at initial pressures of 5–12 bar by Eldeeb and Akih-Kumgeh [42] and the experimental data in a shock tube for DMF/air mixture by Somers et al. [43] at pressures of about 20 and 80 bar and a temperature range of 820–1207 K are taken to assess the proposed mechanism. Figure 5 displays the comparisons between the simulated ignition delays and the measurements. It can be concluded that the ignition delays have an inverse relationship with the pressure. In general, from Figure 5a, the simulated ignition delays obtained by the proposed mechanism satisfied the experimental data at pressures of 5–12 bar. As shown in Figure 5b, the proposed mechanism captures the variation trend of shock tube experimental results at elevated pressures, but a slight discrepancy is observed at temperatures below 850 K; thus, the improvement for the low-temperature chemistry of DMF ought to be carried out sequentially.
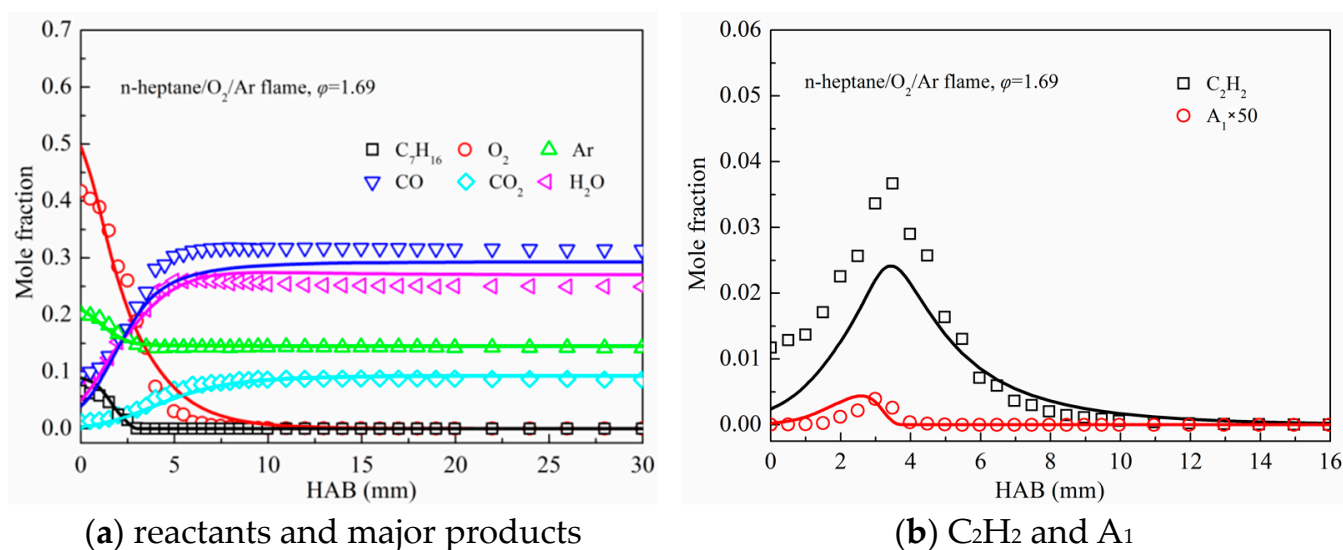
3.2. Premixed Flame Species Profiles

Validations of the present mechanism are also carried out with experimental results in premixed flames available in the literature. The simulation was performed by using PREMIX subroutine from CHEMKIN package [36]. The species formed in a premixed n-heptane flame with φ = 1.69 as a function of the sampling height above the burner (HAB) at a pressure of 40 mbar was investigated by Seidel and his coworkers [44]. Figure 6 compares the experimental results for reactants, major combustion products and two selected intermediate species—given that C_2H_2 and benzene (A_1) play significant roles in forming the multiring PAH molecules—with those simulations of the present mechanism. At the main oxidation zone, both the experimental and predicted results show that the concentrations of major combustion products increase rapidly with the reactants consumed, while the C_2H_2 and A_1 profiles first increase and then decrease rapidly. As the fuel is completely consumed, the main products reach constant mole fraction values above the main oxidation area. In general, the predictions of the reactants, intermediates and major products by the proposed mechanism reasonably match those of the experimental results,

although a small discrepancy between the prediction and measurement exists in the peak concentration of C_2H_2, which is underestimated by about 35.13%.


(**a**) P = 5–12 bar   (**b**) P = 20 and 80 bar

Figure 5. Comparisons between the predicted (lines) and experimental [42,43] (symbols) ignition delays of DMF.

(**a**) reactants and major products   (**b**) C_2H_2 and A_1

Figure 6. Measured [44] (symbols) and predicted (lines) species profiles in premixed n-heptane flame.

An experiment on low-pressure (4.0 kPa) premixed toluene/O_2/Ar flames for $\varphi = 1.0$ and 1.75 was carried out by Li et al. [45], and the species concentration profiles in the two toluene flames were determined by using synchrotron vacuum ultraviolet photoionization mass spectrometry. Experimental data from Li et al. [45] were also taken to assess the performance of the proposed mechanism. Figure 7 presents the measured and predicted mole fraction profiles of reactants, major products (CO, CO_2, H_2 and H_2O) and two selected intermediate species in premixed toluene flames. The results revealed that the present mechanism's simulated species concentrations of reactants and major products meet the experimental results quite well. Furthermore, the proposed mechanism can correctly capture the variation trends of two intermediates (C_2H_2 and A_1), but some disagreements between simulations and experiments are observed below 3 mm above the burner.

(**a**) reactants and major products   (**b**) C_2H_2 and A_1
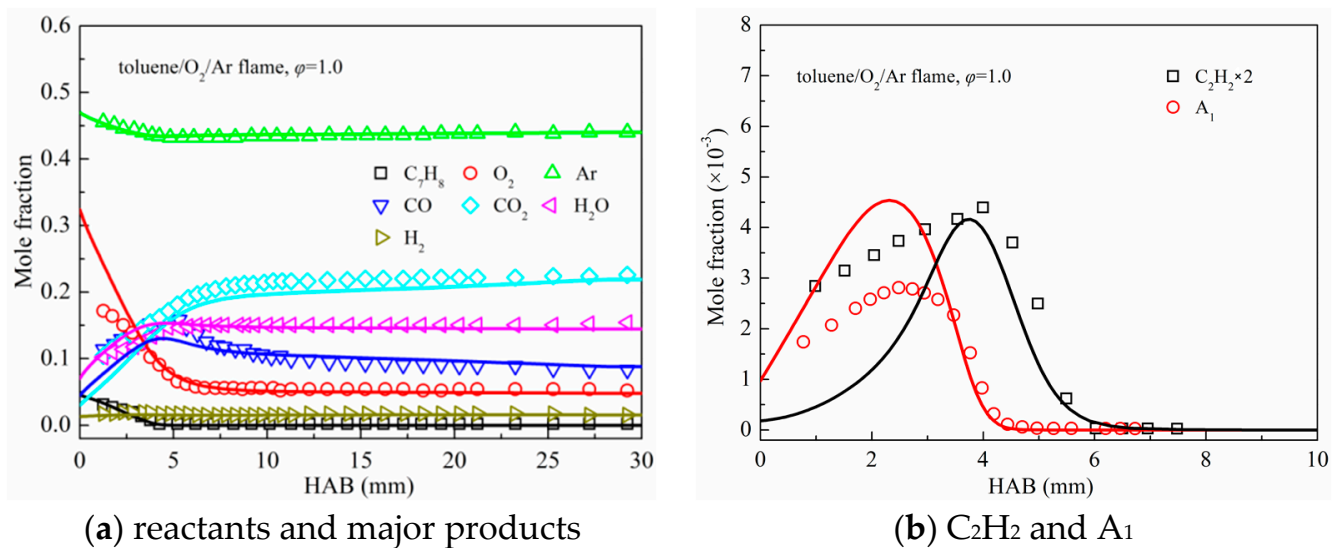
Figure 7. Measured [45] (symbols) and predicted (lines) species profiles in premixed toluene flame.

Knyazkov et al. [46] investigated the speciation data for a premixed fuel-rich ($\varphi = 1.75$) atmospheric pressure n-heptane/toluene mixture (70%:30% by liquid volume) flame by employing molecular beam mass spectrometry. As shown in Figure 8, the proposed mechanism's simulated species concentrations of n-heptane/toluene flame are compared with that of experimental data of reactants, major combustion products and two intermediate species. It is evident from Figure 8a that the proposed mechanism can well reproduce the experimental data of n-heptane, toluene, O_2 and major products (CO, CO_2, H_2 and H_2O). In addition, the present mechanism satisfactorily predicts the A_1 molecule mole fraction (see Figure 8b), but the experimental data of the C_2H_2 mole fraction are not reasonably predicted by the present mechanism. The peak value of the C_2H_2 mole concentrations is obviously overpredicted. Meanwhile, the present mechanism significantly overpredicts the C_2H_2 mole concentration in the post-flame zone compared to the experimental data; similar results were also obtained by Knyazkov et al. [46]. This discrepancy may be due to the lack of some important combustion chemistry of C_2H_2 species in the present mechanism.

(**a**) reactants and major products   (**b**) C_2H_2 and A_1
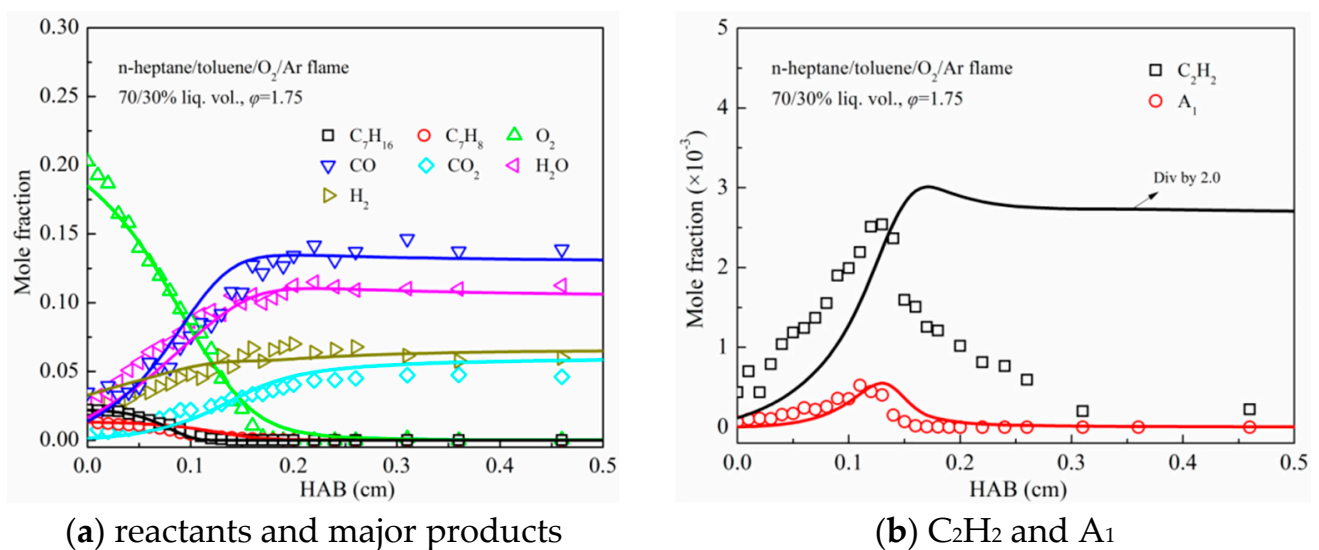
Figure 8. Measured [46] (symbols) and predicted (lines) species profiles in premixed n-heptane/toluene flame.

Togbé et al. [47] investigated a premixed fuel-rich ($\varphi = 1.7$) DMF/O_2/Ar flame at low pressure (40 mbar), and the species concentration profiles were detected using gas

chromatography. In Figure 9, the measured major species—C_2H_2 and A_1—profiles in a DMF premixed flame are compared with those predictions by the proposed mechanism. As observed from Figure 9, the predictions of reactants, CO, H_2O and H_2 agree well with the experimental values. Moreover, the proposed mechanism offers a good description for the C_2H_2 mole fraction, although the prediction is slightly shifted towards the high height of the burner. However, the predicted CO_2 and A_1 profiles are slightly lower than the experimental data, which may be caused by the simplification of the proposed mechanism; such discrepancy can also be found in the work of Togbé et al. [47]. Overall, the predictions of species concentration profiles in the DMF premixed flame are in good agreement with experimental results.

(**a**) reactants and major products　　　　　　　　　　(**b**) C_2H_2 and A_1
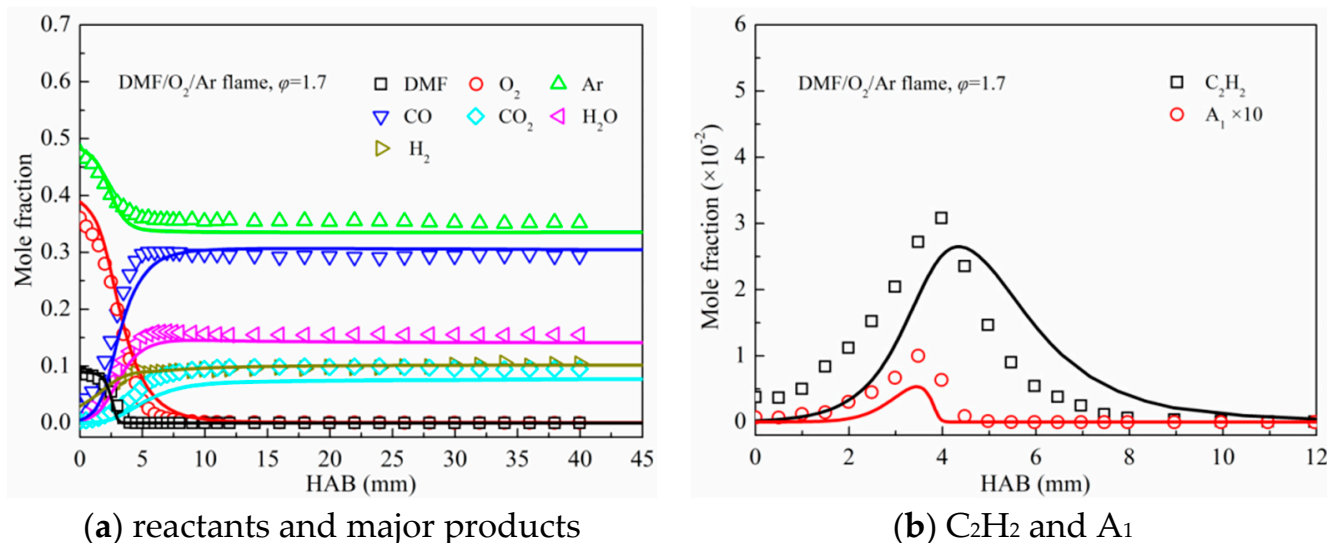
Figure 9. Measured [47] (symbols) and predicted (lines) species profiles in premixed DMF flame.

Larger PAH components are identified as the gaseous precursors of soot particles; although the A1 concentrations in premixed n-heptane, toluene, n-heptane/toluene and DMF flames are reliably predicted using the present mechanism, future validation of PAHs species profiles should be performed. Defoeux et al. [48] experimentally studied the premixed fuel-rich ($\varphi = 2.0$) benzene/O_2/Ar flame at a pressure of 50 mbar. Similarly, Yang et al. [49] determined the PAH species profiles in a premixed benzene/O_2/Ar flame at 4.0 kPa with $\varphi = 1.78$. As shown in Figures 10 and 11, the predicted species mole fraction profiles in two laminar premixed benzene/O_2/Ar flames are compared with those measured data. As can be seen, the measured data of small species and A_1 can be reasonably well reproduced by the proposed mechanism. Moreover, the predicted mole fraction profiles of naphthalene (A_2), acenaphthylene (A_2R_5), phenanthrene (A_3) and pyrene (A_4) are also acceptable in comparison to the measured data, which indicates that the chemical reaction pathways of PAH formation and consumption involving the proposed mechanism are reliable.

3.3. Engine Combustion Validation

In this section, new diesel engine experiments were performed on a four-cylinder CI engine, experimental data for in-cylinder combustion characteristics and engine-out emissions are also taken to verify the reduced n-heptane/toluene/DMF-PAH mechanism. Detailed descriptions of the experimental setup and the measurement uncertainties can be found in [10,50]. Table 3 lists the engine specifications and the experimental conditions. In the experiments, pure diesel and DMF30 (mixture of 70% diesel and 30% DMF by mass) were used and directly delivered into the cylinder via a common-rail high-pressure DI injector located in the center of the cylinder head with seven nozzles. The injection timings for pure diesel and DMF30 were both fixed at a 7.5 crank angle (CA) before top dead center

(BTDC). The in-cylinder pressure data were obtained by a pressure transducer (Kistler 6052C). Soot and NOx emissions were detected utilizing a particle analyzer (DMS500) and an AVL emission analyzer, respectively.

(**a**) A_1, C_2H_2 and C_2H_4 (**b**) large PAH molecules
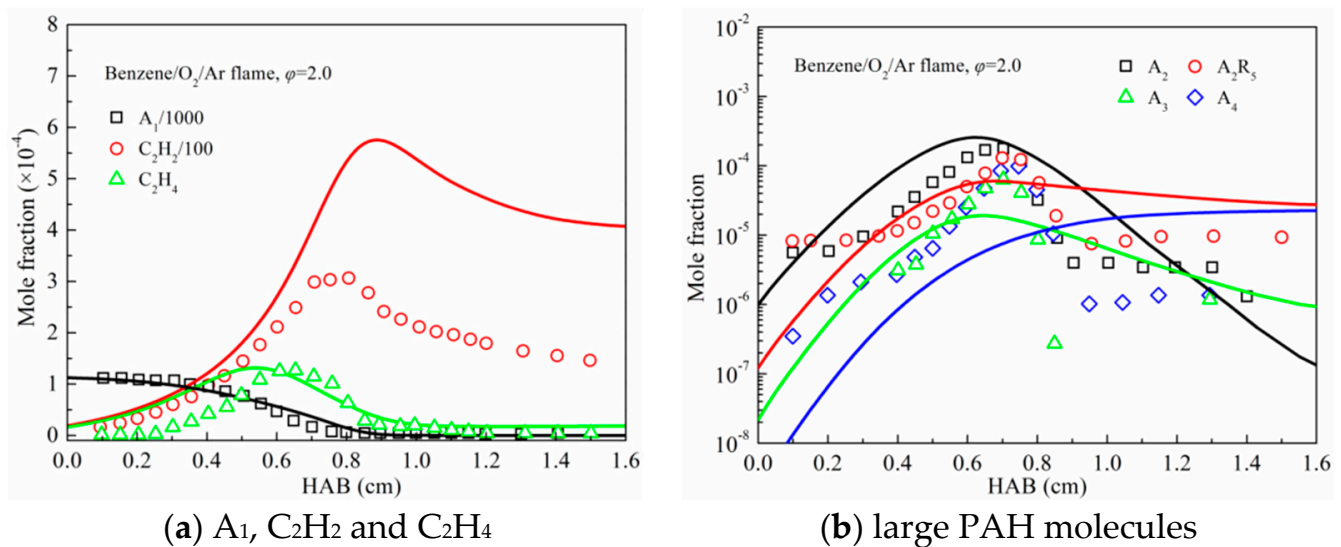
Figure 10. Measured [48] (symbols) and predicted (lines) species profiles in the premixed benzene flame with φ = 2.0.

(**a**) A_1, C_2H_2 and C_4H_2 (**b**) large PAH molecules
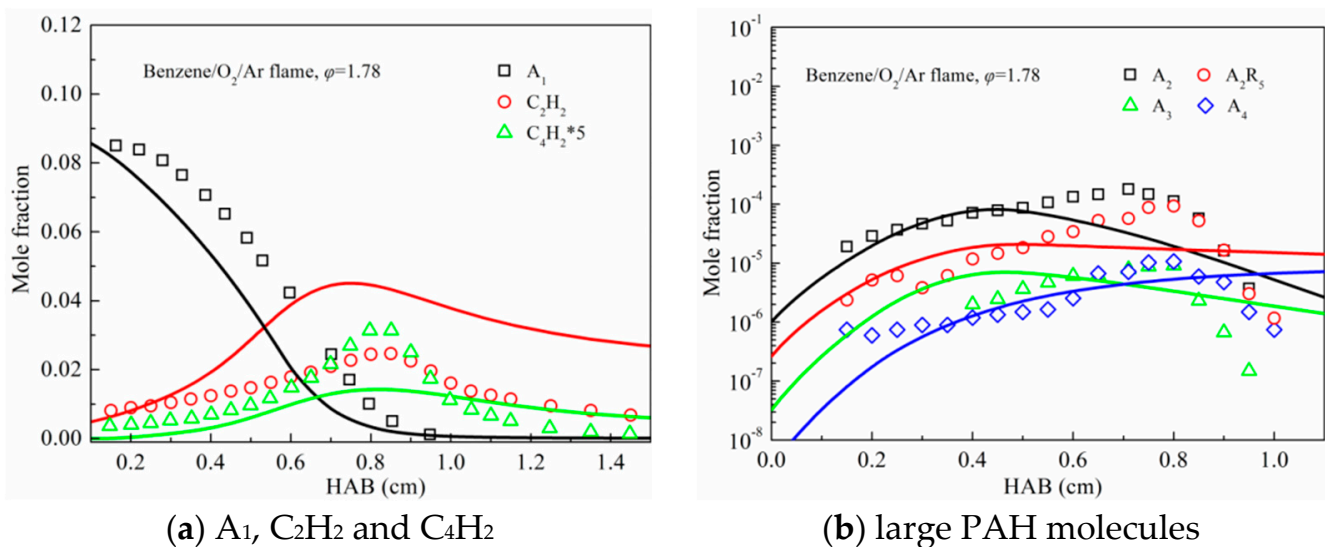
Figure 11. Measured [49] (symbols) and predicted (lines) species profiles in the premixed benzene flame with φ = 1.78.

The multidimensional engine simulations were performed by KIVA-CHEMKIN code [51]. As shown in Figure 12, a 51.4286° computational grid generated using the preprocessor of the KIVA was used to carry out the simulations. The combustion chemistry of diesel was modeled with the n-heptane and toluene submechanism [28], and the physical properties of diesel were modeled by n-tetradecane. For the DMF fuel, its own physical properties and chemistry reaction mechanism were used. The KH-RT model was adopted to model the fuel injection and spray droplet breakup. The turbulent flow was simulated by the RNG k-ε model. A reduced NOx mechanism derived from [52] was coupled with the proposed mechanism to model NOx formation. Soot emissions were predicted using an improved multistep soot model [28].

Table 3. Engine specifications and operating conditions.

Engine Name	YC4FA115-40
Cylinders	4 in-line
Capacity	2.982 L
Compression ratio	17.5:1
Bore × Stroke	96 mm × 103 mm
Connecting rod length	115 mm
Fuel injection system	High-pressure common-rail
Number of holes	7
Inlet valve close	−133 CA ATDC
Exhaust valve open	125 CA ATDC
Engine speed	1800 r/min
Brake mean effective pressure	~0.60 MPa
Intake air temperature	288 K
Intake air pressure	1.25 bar
Common-rail pressure	110 MPa
Injection timing	7.5 CA BTDC
EGR	none
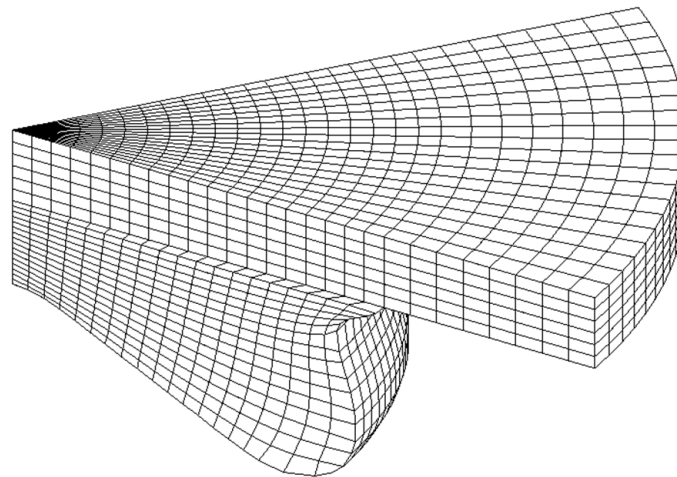
Figure 12. Computational mesh.

Figure 13 depicts the simulated in-cylinder pressure and HRR histories for pure diesel and DMF30 against the experimental data. As seen, the combustion process of the diesel fuel consists of two heat release phases, but the two-stage heat release pattern becomes unobvious for DMF30, which means the proportion of premixed combustion is increased. Compared to the diesel fuel, DMF has lower cetane number, higher autocombustion temperature and higher latent heat of vaporization; thus, the start of heat release for DMF30 fuel is prolonged. The longer ignition delay of DMF30 results in more premixed combustion and higher peak pressure compared to pure diesel. Generally, the predicted in-cylinder pressures and HRRs for diesel and DMF30 agree well with the measured results, which indicates that the present mechanism can be employed for multidimensional diesel engine combustion simulations.

Figure 14 displays the simulated results of soot and NOx emissions using the present mechanism against the experiments. As seen, both simulated and experimental data indicate that the soot emission level of diesel is obviously higher than DMF30 as there is more carbon content and less oxygen content in the diesel fuel, while DMF30 produces more NOx emissions compared with diesel due to the enhanced premixed combustion, which is consistent with other studies [14,23]. In general, the predicted soot and NOx emissions are fairly close to the experimental data, considering the existing experimental error and the size of the proposed mechanism.
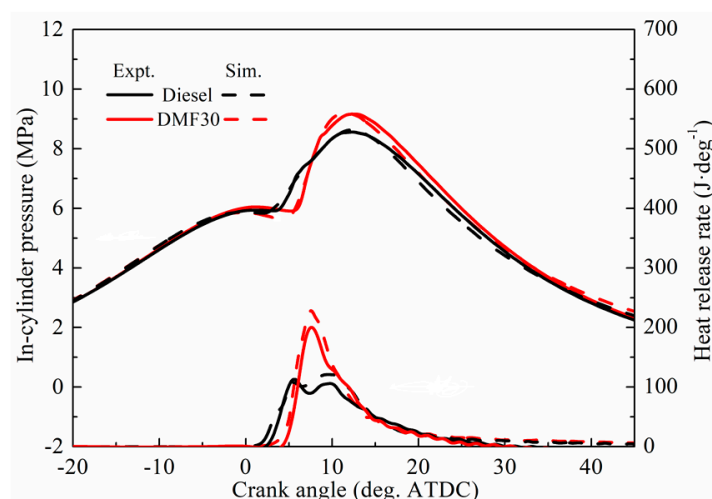
Figure 13. Measured and predicted in-cylinder pressure and HRR profiles.
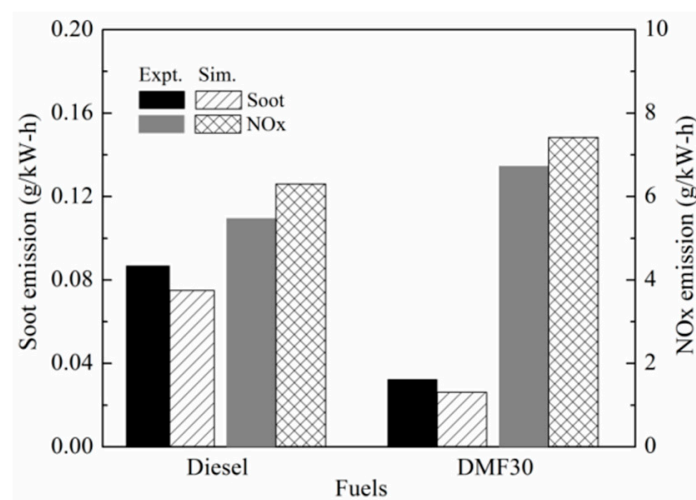

Figure 14. Measured and predicted soot and NOx emission profiles.

4. Conclusions

In this work, a reduced n-heptane/toluene/DMF-PAH reaction mechanism comprising only 78 species and 190 reactions has been developed for diesel/DMF engine applications. A detailed DMF mechanism was firstly reduced using DRGER, CSP, ROPA, SA and chemical lumping methods. Thereafter, a combined mechanism was constructed by integrating the obtained reduced DMF mechanism with a skeletal diesel surrogate model with PAH formation proposed in our previous work. The reduced three-component reaction mechanism was finally formed after optimizing the rate constants of some significant reactions. The newly proposed three-component reaction mechanism was extensively assessed by comparison with available experimental results of ignition delay and premixed flame species concentrations. Moreover, experimental data of in-cylinder pressure, HRR, soot and NOx emissions from new diesel engine experiments were used for evaluating the reduced mechanism. Validation results showed that the proposed mechanism can give fairly good predictions on the experimental data. In conclusion, this novel reduced n-heptane/toluene/DMF-PAH mechanism can be utilized to predict the combustion and emissions of diesel engines fueled with diesel and DMF fuels.

Supplementary Materials: The following supporting information can be downloaded at: https://www.mdpi.com/article/10.3390/atmos14040642/s1, S1: chem.inp; S2: therm.dat.

Institutional Review Board Statement: Not applicable.

Informed Consent Statement: Not applicable.

Data Availability Statement: Not applicable.

Conflicts of Interest: The authors declare no conflict of interest.

References

1. Singh, R.; Singh, S.; Kumar, M. Impact of n-butanol as an additive with eucalyptus biodiesel-diesel blends on the performance and emission parameters of the diesel engine. *Fuel* **2020**, *277*, 118178. [CrossRef]
2. Vijay Kumar, M.; Veeresh Babu, A.; Ravi Kumar, P.; Sudhakara Reddy, S. Experimental investigation of the combustion characteristics of mahua oil biodiesel-diesel blend using a di diesel engine modified with egr and nozzle hole orifice diameter. *Biofuel Res. J.* **2018**, *5*, 863–871. [CrossRef]
3. Alexandrino, K. Comprehensive review of the impact of 2,5-dimethylfuran and 2-methylfuran on soot emissions: Experiments in diesel engines and at laboratory-scale. *Energy Fuels* **2020**, *34*, 6598–6623. [CrossRef]
4. Channappagoudra, M.; Ramesh, K.; Manavendra, G. Comparative investigation of the effect of hemispherical and toroidal piston bowl geometries on diesel engine combustion characteristics. *Biofuel Res. J.* **2018**, *5*, 854–862. [CrossRef]
5. Wang, H.; Deneys Reitz, R.; Yao, M.; Yang, B.; Jiao, Q.; Qiu, L. Development of an n-heptane-n-butanol-pah mechanism and its application for combustion and soot prediction. *Combust. Flame* **2013**, *160*, 504–519. [CrossRef]
6. Zhong, S.; Daniel, R.; Xu, H.; Zhang, J.; Turner, D.; Wyszynski, M.L.; Richards, P. Combustion and emissions of 2, 5-dimethylfuran in a direct-injection spark-ignition engine. *Energy Fuels* **2010**, *24*, 2891–2899. [CrossRef]
7. Shukla, M.K.; Singh, E.; Singh, N.; Singal, S.K. Prospects of 2,5-dimethylfuran as a fuel: Physico-chemical and engine performance characteristics evaluation. *J. Mater. Cycles Waste Manag.* **2015**, *17*, 459–464. [CrossRef]
8. Zheng, Z.; Wang, X.; Yue, L.; Liu, H.; Yao, M. Effects of six-carbon alcohols, ethers and ketones with chain or ring molecular structures on diesel low temperature combustion. *Energy Convers. Manag.* **2016**, *124*, 480–491. [CrossRef]
9. Xiao, H.; Hou, B.; Zeng, P.; Jiang, A.; Hou, X.; Liu, J. Combustion and emission characteristics of diesel engine fueled with 2,5-dimethylfuran and diesel blends. *Fuel* **2017**, *192*, 53–59. [CrossRef]
10. Wei, M.; Li, S.; Liu, J.; Guo, G.; Sun, Z.; Xiao, H. Effects of injection timing on combustion and emissions in a diesel engine fueled with 2,5-dimethylfuran-diesel blends. *Fuel* **2017**, *192*, 208–217. [CrossRef]
11. Wei, M.; Li, S.; Xiao, H.; Guo, G. A comparison study on the combustion and particulate emissions of 2,5-dimethylfuran/diesel and ethanol/diesel in a diesel engine. *Therm. Sci.* **2018**, *22*, 1351–1361. [CrossRef]
12. Saha, B.; Abu-Omar, M.M. Current technologies economics and perspectives for 2,5-dimethylfuran production from biomass-derived intermediates. *ChemSusChem* **2015**, *8*, 1133–1142. [CrossRef]
13. Hu, L.; Jiang, Y.; Xu, J.; He, A.; Wu, Z.; Xu, J. Chemocatalytic pathways for high-efficiency production of 2,5-dimethylfuran from biomass-derived 5-hydroxymethylfurfural. In *Biomass, Biofuels, Biochemicals*; Elsevier: Amsterdam, The Netherlands, 2020; pp. 377–394.
14. Liu, X.; Wang, H.; Wei, L.; Liu, J.; Reitz, R.D.; Yao, M. Development of a reduced toluene reference fuel (TRF)-2,5-dimethylfuran-polycyclic aromatic hydrocarbon (PAH) mechanism for engine applications. *Combust. Flame* **2016**, *165*, 453–465. [CrossRef]
15. Zheng, Z.; Wang, X.; Zhong, X.; Hu, B.; Liu, H.; Yao, M. Experimental study on the combustion and emissions fueling biodiesel/n-butanol, biodiesel/ethanol and biodiesel/2,5-dimethylfuran on a diesel engine. *Energy* **2016**, *115*, 539–549. [CrossRef]
16. Daniel, R.; Tian, G.; Xu, H.; Wyszynski, M.L.; Wu, X.; Huang, Z. Effect of spark timing and load on a disi engine fuelled with 2,5-dimethylfuran. *Fuel* **2011**, *90*, 449–458. [CrossRef]
17. Daniel, R.; Wei, L.; Xu, H.; Wang, C.; Wyszynski, M.L.; Shuai, S. Speciation of hydrocarbon and carbonyl emissions of 2,5-dimethylfuran combustion in a disi engine. *Energy Fuels* **2012**, *26*, 6661–6668. [CrossRef]
18. Rothamer, D.A.; Jennings, J.H. Study of the knocking propensity of 2,5-dimethylfuran–Gasoline and ethanol–Gasoline blends. *Fuel* **2012**, *98*, 203–212. [CrossRef]
19. Wang, C.; Xu, H.; Herreros, J.M.; Lattimore, T.; Shuai, S. Fuel effect on particulate matter composition and soot oxidation in a direct-injection spark ignition (DISI) engine. *Energy Fuels* **2014**, *28*, 2003–2012. [CrossRef]

20. Zhang, Q.; Chen, G.; Zheng, Z.; Liu, H.; Xu, J.; Yao, M. Combustion and emissions of 2,5-dimethylfuran addition on a diesel engine with low temperature combustion. *Fuel* **2013**, *103*, 730–735. [CrossRef]

21. Chen, G.; Shen, Y.; Zhang, Q.; Yao, M.; Zheng, Z.; Liu, H. Experimental study on combustion and emission characteristics of a diesel engine fueled with 2,5-dimethylfuran–Diesel, n-butanol–Diesel and gasoline–Diesel blends. *Energy* **2013**, *54*, 333–342. [CrossRef]

22. Chen, G.; Di, L.; Zhang, Q.; Zheng, Z.; Zhang, W. Effects of 2,5-dimethylfuran fuel properties coupling with egr (exhaust gas recirculation) on combustion and emission characteristics in common-rail diesel engines. *Energy* **2015**, *93*, 284–293. [CrossRef]

23. Liu, H.; Xu, J.; Zheng, Z.; Li, S.; Yao, M. Effects of fuel properties on combustion and emissions under both conventional and low temperature combustion mode fueling 2,5-dimethylfuran/diesel blends. *Energy* **2013**, *62*, 215–223. [CrossRef]

24. Xiao, H.; Zeng, P.; Zhao, L.; Li, Z.; Fu, X. An experimental study of the combustion and emission performances of 2,5-dimethylfuran diesel blends on a diesel engine. *Therm. Sci.* **2017**, *21*, 543–553. [CrossRef]

25. Wang, X.; Wang, Y.; Bai, Y.; Wang, P.; Wang, D.; Guo, F. Effects of 2,5-dimethylfuran addition on morphology, nanostructure and oxidation reactivity of diesel exhaust particles. *Fuel* **2019**, *253*, 731–740. [CrossRef]

26. Weber, J.; Won, H.; Peters, N. *Experimental Validation of a Surrogate Fuel for Diesel*; No. 2007-01-1842, SAE Technical Paper; SAE: Warrendale, PA, USA, 2007.

27. Tran, L.S.; Sirjean, B.; Glaude, P.A.; Kohse-Höinghaus, K.; Battin-Leclerc, F. Influence of substituted furans on the formation of polycyclic aromatic hydrocarbons in flames. *Proc. Combust. Inst.* **2015**, *35*, 1735–1743. [CrossRef]

28. Li, S.; Li, Y.; Liu, J.; Meng, W.; Wang, M.; Cao, Y.; Cao, S.; Yao, L.; Zhang, K. Development of a phenomenological soot model integrated with a reduced trf-pah mechanism for diesel engine application. *Fuel* **2021**, *283*, 118810. [CrossRef]

29. Pepiot-Desjardins, P.; Pitsch, H. An efficient error-propagation-based reduction method for large chemical kinetic mechanisms. *Combust. Flame* **2008**, *154*, 67–81. [CrossRef]

30. Lu, T.; Law, C.K. Strategies for mechanism reduction for large hydrocarbons: N-heptane. *Combust. Flame* **2008**, *154*, 153–163. [CrossRef]

31. Fredriksson, J.; Bergman, M.; Golovitchev, V.I.; Denbratt, I. *Modeling the Effect of Injection Schedule Change on Free Piston Engine Operation*; No. 2006-01-0449, SAE Technical Paper; SAE: Warrendale, PA, USA, 2006.

32. Golovitchev, V.; Calik, A.; Montorsi, L. *Analysis of Combustion Regimes in Compression Ignited Engines Using Parametric Φ-T Dynamic Maps*; No. 2007-01-1838, SAE Technical Paper; SAE: Warrendale, PA, USA, 2007.

33. Cancino, L.R.; Fikri, M.; Oliveira, A.A.M.; Schulz, C. Autoignition of gasoline surrogate mixtures at intermediate temperatures and high pressures: Experimental and Numerical Approaches. *Proc. Combust. Inst.* **2009**, *32*, 501–508. [CrossRef]

34. Chang, Y.; Jia, M.; Li, Y.; Liu, Y.; Xie, M.; Wang, H.; Reitz, R.D. Development of a skeletal mechanism for diesel surrogate fuel by using a decoupling methodology. *Combust. Flame* **2015**, *162*, 3785–3802. [CrossRef]

35. Andrae, J.C.G.; Björnbom, P.; Cracknell, R.F.; Kalghatgi, G.T. Autoignition of toluene reference fuels at high pressures modeled with detailed chemical kinetics. *Combust. Flame* **2007**, *149*, 2–24. [CrossRef]

36. Kee, R.J.; Rupley, F.M.; Miller, J.A. *CHEMKIN II: A Fortran Chemical Kinetics Package for the Analysis of Gas-Phase Chemical Kinetics*; Sandia Laboratories Report, S. 89-8009B; Sandia National Laboratories: Albuquerque, NM, USA, 1989.

37. Ciezki, H.K.; Adomeit, G. Shock-tube investigation of self-ignition of n-heptane-air mixtures under engine relevant conditions. *Combust. Flame* **1993**, *93*, 421–433. [CrossRef]

38. Hartmann, M.; Gushterova, I.; Fikri, M.; Schulz, C.; Schießl, R.; Maas, U. Auto-ignition of toluene-doped n-heptane and iso-octane/air mixtures: High-pressure shock-tube experiments and kinetics modeling. *Combust. Flame* **2011**, *158*, 172–178. [CrossRef]

39. Davidson, D.F.; Gauthier, B.M.; Hanson, R.K. Shock tube ignition measurements of iso-octane/air and toluene/air at high pressures. *Proc. Combust. Inst.* **2005**, *30*, 1175–1182. [CrossRef]

40. Shen, H.P.S.; Vanderover, J.; Oehlschlaeger, M.A. A shock tube study of the auto-ignition of toluene/air mixtures at high pressures. *Proc. Combust. Inst.* **2009**, *32*, 165–172. [CrossRef]

41. Herzler, J.; Fikri, M.; Hitzbleck, K.; Starke, R.; Schulz, C.; Roth, P.; Kalghatgi, G.T. Shock-tube study of the autoignition of n-heptane/toluene/air mixtures at intermediate temperatures and high pressures. *Combust. Flame* **2007**, *149*, 25–31. [CrossRef]

42. Eldeeb, M.A.; Akih-Kumgeh, B. Reactivity trends in furan and alkyl furan combustion. *Energy Fuels* **2014**, *28*, 6618–6626. [CrossRef]

43. Somers, K.P.; Simmie, J.M.; Gillespie, F.; Conroy, C.; Black, G.; Metcalfe, W.K.; Battin-Leclerc, F.; Dirrenberger, P.; Herbinet, O.; Glaude, P.A.; et al. A comprehensive experimental and detailed chemical kinetic modelling study of 2,5-dimethylfuran pyrolysis and oxidation. *Combust. Flame* **2013**, *160*, 2291–2318. [CrossRef]

44. Seidel, L.; Moshammer, K.; Wang, X.; Zeuch, T.; Kohse-Höinghaus, K.; Mauss, F. Comprehensive kinetic modeling and experimental study of a fuel-rich, premixed n-heptane flame. *Combust. Flame* **2015**, *162*, 2045–2058. [CrossRef]

45. Li, Y.; Cai, J.; Zhang, L.; Yuan, T.; Zhang, K.; Qi, F. Investigation on chemical structures of premixed toluene flames at low pressure. *Proc. Combust. Inst.* **2011**, *33*, 593–600. [CrossRef]

46. Knyazkov, D.A.; Slavinskaya, N.A.; Dmitriev, A.M.; Shmakov, A.G.; Korobeinichev, O.P.; Riedel, U. Structure of an n-heptane/toluene flame: Molecular beam mass spectrometry and computer simulation investigations. *Combust Explos Shock Waves* **2016**, *52*, 142–154. [CrossRef]

47. Togbé, C.; Tran, L.S.; Liu, D.; Felsmann, D.; Oßwald, P.; Glaude, P.A.; Sirjean, B.; Fournet, R.; Battin-Leclerc, F.; Kohse-Höinghaus, K. Combustion chemistry and flame structure of furan group biofuels using molecular-beam mass spectrometry and gas chromatography—Part iii: 2,5-dimethylfuran. *Combust. Flame* **2014**, *161*, 780–797. [CrossRef] [PubMed]
48. Defoeux, F.; Dias, V.; Renard, C.; Van Tiggelen, P.J.; Vandooren, J. Experimental investigation of the structure of a sooting premixed benzene/oxygen/argon flame burning at low pressure. *Proc. Combust. Inst.* **2005**, *30*, 1407–1415. [CrossRef]
49. Yang, B.; Li, Y.; Wei, L.; Huang, C.; Wang, J.; Tian, Z.; Yang, R.; Sheng, L.; Zhang, Y.; Qi, F. An experimental study of the premixed benzene/oxygen/argon flame with tunable synchrotron photoionization. *Proc. Combust. Inst.* **2007**, *31*, 555–563. [CrossRef]
50. Li, S.; Liu, J.; Li, Y.; Wei, M.; Xiao, H.; Yang, S. Effects of fuel properties on combustion and pollutant emissions of a low temperature combustion mode diesel engine. *Fuel* **2020**, *267*, 117123. [CrossRef]
51. Amsden, A.A. *KIVA-3V, Release 2: Improvements to KIVA-3V*; Los Alamos National Laboratory Report LA-UR-99-915; Los Alamos National Laboratory: Santa Fe, NM, USA, 1999.
52. Kong, S.C.; Sun, Y.; Rietz, R.D. Modeling diesel spray flame liftoff, sooting tendency, and nox emissions using detailed chemistry with phenomenological soot model. *J. Eng. Gas Turbines Power* **2007**, *129*, 245–251. [CrossRef]